BaCoO 2 with Tetrahedral Cobalt Coordination: The Missing Element to Understand Energy Storage and Conversion Applications in BaCoO 3–δ -Based Materials

Aliou Diatta, Claire Colin, Romain Viennois, Mickael Beaudhuin, Julien Haines, Patrick Hermet, Arie van der Lee, Leszek Konczewicz, Pascale Armand, Jérôme Rouquette

$BaCoO_2$ with tetrahedral cobalt-coordination: The Missing Element to understand Energy Storage and Conversion Applications in Ba-$CoO_{3-\delta}$-based-Materials

Aliou Diatta, Claire V. Colin, Romain Viennois, Mickael Beaudhuin, Julien Haines, Patrick Hermet, Arie van der Lee, Leszek Konczewicz, Pascale Armand and Jérôme Rouquette*

ICGM, Univ Montpellier, CNRS, ENSCM, Montpellier, France

Institut Néel, CNRS and Université Grenoble Alpes, BP166, F-38042 Grenoble Cedex 9, France

IEM, Univ Montpellier, CNRS, ENSCM, Montpellier, France

L2C, Univ Montpellier, CNRS, Montpellier, France

Institut of High Pressure Physics, Polish Academy of Sciences, Sokołowska 29/37, 01-142 Warsaw, Poland.

KEYWORDS

ABSTRACT: Barium-cobaltate-based perovskite ($BaCoO_{3-\delta}$) and barium-cobaltate-based nanocomposites have been intensively studied in energy storage and conversion devices mainly due to flexible oxygen stoichiometry and tunable non-precious transition metal oxidation states. Although a rich and complex family of structural polymorphs has already been reported for these perovskites in the literature, the potential structural evolution which may occur during the oxygen reduction reaction and the oxygen evolution reaction has not been investigated so far. In this study, we synthetized and characterized the lowest Co-oxidation state possible in the compound, $BaCoO_2$, which exhibits a quartz-derived, trigonal structure with a helicoidally corner-sharing, CoO_4-tetrahedral-framework as already proposed by Spitsbergen et al. Oxygen can reversibly be inserted in such a crystal structure to form $BaCoO_{3-\delta}$, i.e. with $0 \leq \delta \leq 1$, based on the results of an *in-situ* coupled thermogravimetric - neutron diffraction study and which presents therefore giant oxygen capacity storage due to the extreme tunability of the electronic configuration of the cobalt cations which defines the fundamental origins of the materials performance. The reversible conversion of $BaCoO_2$ to $BaCoO_{3-\delta}$ associated with a similar electronic conductivity above 900 K permits to clarify the high potential of $BaCoO_{3-\delta}$ -based energy storage and conversion devices.

INTRODUCTION

Energy storage and conversion devices are nowadays necessary to be coupled with renewable energy solutions (solar, wind) in order to efficiently reduce carbon dioxide emissions and potentially achieve carbon neutrality. ABO_3 perovskite oxides using non-precious metals appear as an interesting solution for such a goal as they present the advantage of being cheap and they possess high catalytic performance as electrode materials[1-5]. These performances mainly arise from the ability from the perovskite crystal structure to exhibit an outstanding tunable oxygen stoichiometry due to the existence of oxygen vacancies[6,7] which means that oxygen can reversibly be inserted and released in the framework depending on the oxygen partial pressure pO_2 and temperature, for example. Perovskite oxides have to exhibit therefore mixed oxygen-ion and electron conductor properties for applications as electrodes for ceramic fuel cells, catalysts for water splitting, oxygen permeation membranes and other advanced oxidation processes.

$BaCoO_{3-\delta}$ (BCO) is found to be present either individually in efficient nanocomposites[8-12] or as a parent phase like in the well-known $Ba_{0.5}Sr_{0.5}Co_{0.8}Fe_{0.2}O_{3-\delta}$ (BSCF) based-perovskite[13] for many of the different catalyst- and electrode-based applications as it presents an exceptional oxygen permeation rate. However, BCO exhibits a distorted hexagonal perovskite structure[14] with face sharing CoO_6 octahedra due to the large differences in the ionic radii[15] of Ba and Co according to the Goldschmidt tolerance factor and as observed in the case of BSCF, it is generally mixed with additional elements[16,17] to stabilize the prototype cubic perovskite[13], Fig. S1. Cubic $BaCoO_{2.2}$ has been documented in the literature with a tolerance factor being adjusted to 1 due to the combination of large Ba^{2+} and $Co^{2/3+}$ ions in the A and B sites[18]. In such a system, the structural instability appears therefore to arise from oxygen vacancies and change in the electronic configuration of cobalt cations. In the BSCF cubic perovskite, for example, which is

known as the standard material in solid oxide fuel cell cathodes[19] and which exhibits excellent oxygen evolution reaction electrocatalyst properties[1], the oxygen non-stoichiometry δ can be varied from 0.2 to 0.8[20,21] due to the versatility in the electronic configuration of the Co/Fe metallic cations on the *B*-perovskite site, i.e. oxidation-, spin- and magnetic-state, which defines the fundamental origins of the material's performance. This cubic perovskite was found not to be very stable in the entire temperature range of applications as it can partially decompose into different hexagonal phases related to BCO[22-24]. Additionally, cubic perovskites, such as BSCF, generally present excessive thermal expansion,[25] which could potentially restrain their applications. To overcome these potential drawbacks, another strategy was reported using BCO-based nanocomposites bringing the corresponding optimal oxygen/electron conduction of hexagonal-perovskite BCO to the cubic-perovskite nanostructures[8-12].

While the BCO system is recognized for its intricate complexity, it prompts speculation about potential connections with the previously mentioned reduced cubic [18]$BaCoO_{2.2}$ and $BaCoO_2$[26] proposed by Spitsbergen et al. This raises the tantalizing possibility of introducing and releasing a complete oxygen atom within the BCO system, offering significant implications for energy storage and conversion devices. In our present study, we have successfully synthesized an almost-pure trigonal phase of $BaCoO_2$ and comprehensively characterized it. Through an *in-situ* combined thermogravimetric (TGA)-neutron diffraction experiment, we have provided evidence for the reversible insertion-release of oxygen, highlighting a substantial oxygen storage capacity in BCO. Moreover, our investigation reveals structural modifications in the cobalt coordination environment with transitions from tetrahedral to octahedral configurations via reconstructive transformations. Notably, an unexpectedly high-temperature antiferromagnetic order was observed *in-situ* for the hexagonal phase of BCO, closely resembling that reported in the BSCF perovskite. These findings highlight the versatility of hexagonal BCO perovskites in energy conversion and storage applications, challenging the notion that only cubic perovskite materials are suitable for such purposes.

EXPERIMENTAL SECTION

Materials. $BaCoO_2$ powder was prepared by a solid-state reaction starting from a stoichiometric mixture of $BaCO_3$ (Aldrich > 99%) and CoO (Alfa Aesar 99.8%) pressed in a 13 mm diameter pellet and heated at 1273 K under a secondary vacuum (about 10^{-6} mbar) for 3 h. After cooling the pellet was crushed and two additional cycles under the same conditions were performed in order to obtain the $BaCoO_2$ material.

Structural and TGA characterization. The 2H-$BaCoO_{3-\delta}$ powdered material was synthesized from a stoichiometric mixture of $BaCO_3$ and CoO under an oxygen flux (PO_2 = 1 bar) at 993 K for 4 hours and quenched in liquid nitrogen.

X-ray powder diffraction using Cu-K_α radiation with a PANalytical XPert diffractometer in Bragg-Brentano geometry equipped with an XCelerator detector was used for phase identification for the sample in air.

Transmission geometry using Si (111) monochromator (Cu-$K_{\alpha 1}$ wavelength) was used to appropriately characterize the $BaCoO_2$/BCO powder loaded into a 0.5 mm glass capillary. The structures were refined using the Rietveld method with the programs of the FULLPROF suite[27].

High-temperature X-ray powder diffraction measurements in air were obtained on a PANalytical X'Pert diffractometer equipped with an X'Celerator detector in Bragg-Brentano geometry using Cu-K_α radiation. The $BaCoO_2$ powder was placed in the ceramic spinning sample holder of an Anton Paar HTK 1200 high-temperature oven-chamber.

TGA measurements were performed using a STA-449 F1 Jupiter analyzer (NETZSCH) in air or under a vacuum of 10^{-6} mbar.

Neutron powder diffraction measurements were performed at the D1B diffractometer at the ILL neutron source in Grenoble, France[28] from a sample contained in a glassy silica (covered with gold foils to avoid reaction between $BaCoO_2$ and the amorphous crucible) or vanadium can, placed into a high temperature furnace (with a theoretical maximum temperature of 1273 K) in air or under a vacuum of 5.10^{-5}-10^{-6} mbar. A monochromatic neutron beam with a wavelength of 2.52 Å, obtained with a HOPG monochromator was used. The structural data was refined using the Rietveld method and the Bond Valence Sum (BVS) was calculated with the programs of the FULLPROF suite[27].

Raman Spectroscopy. Raman spectra were collected using a Horiba Jobin-Yvon LabRam Aramis Raman spectrometer incorporating a blue diode laser with a wavelength of 473 nm, an Olympus microscope, and a charge-coupled device camera cooled by a thermoelectric Peltier device. The laser power directed onto the sample was approximately 1 mW. A $BaCoO_2$ pellet was positioned in air on a slender platinum block within the oven of a Linkam TS1500 heating stage beneath the microscope's objective lens (magnification: 50×).

Computational details. The dynamical matrix and normal modes of vibrations at the zone center are calculated, via the knowledge of Hellmann-Feynman forces, in the harmonic approximation using the direct method with an atomic displacement of 0.02 Å. All calculations are spin-polarized in the ferromagnetic state and have been performed with VASP code[29,30]. The volume was fixed to the experimental one and atomic positions were relaxed until the maximum residual forces on each atom are less than 0.003 eV.$Å^{-1}$. Exchange-correlation effects are handled within the generalized gradient approximation (GGA) as proposed by Perdew, Burke and Ernzerhof[31]. The interactions between ions and electrons are described by the projector augmented wave method[32]. The plane wave energy cutoff was 650 eV and the Brillouin zone integration was performed using a 8x8x8 Monkhorst-Pack mesh[33]. To properly describe the strong electron correlations in Co-atoms, a Hubbard term (U_{eff} = 3.4 eV) has been considered as formulated by Dudarev *et al.*[34]. Position of the Raman lines has been determined via the group theory from the knowledge of the eigenmodes obtained by the diagonalization of the dynamical matrix.

RESULTS AND DISCUSSION

From $BaCoO_2$

In spite of its importance in energy storage and conversion devices, the $BaCoO_{3-\delta}$ oxygen-based system is not so well understood. Different polymorphs[35] were reported depending on the oxygen stoichiometry: from the hexagonal $BaCoO_{3-\delta}$ perovskite[14] to the modified 12H- hexagonal[36] and 5H- trigonal phases[37] for oxygen-rich compositions, whereas a strongly oxygen-deficient $BaCoO_{2.2}$ cubic perovskite structure[18] and the end-membered trigonal $BaCoO_2$ were proposed as the reduced phases. The latter phase is proposed to have a quartz-

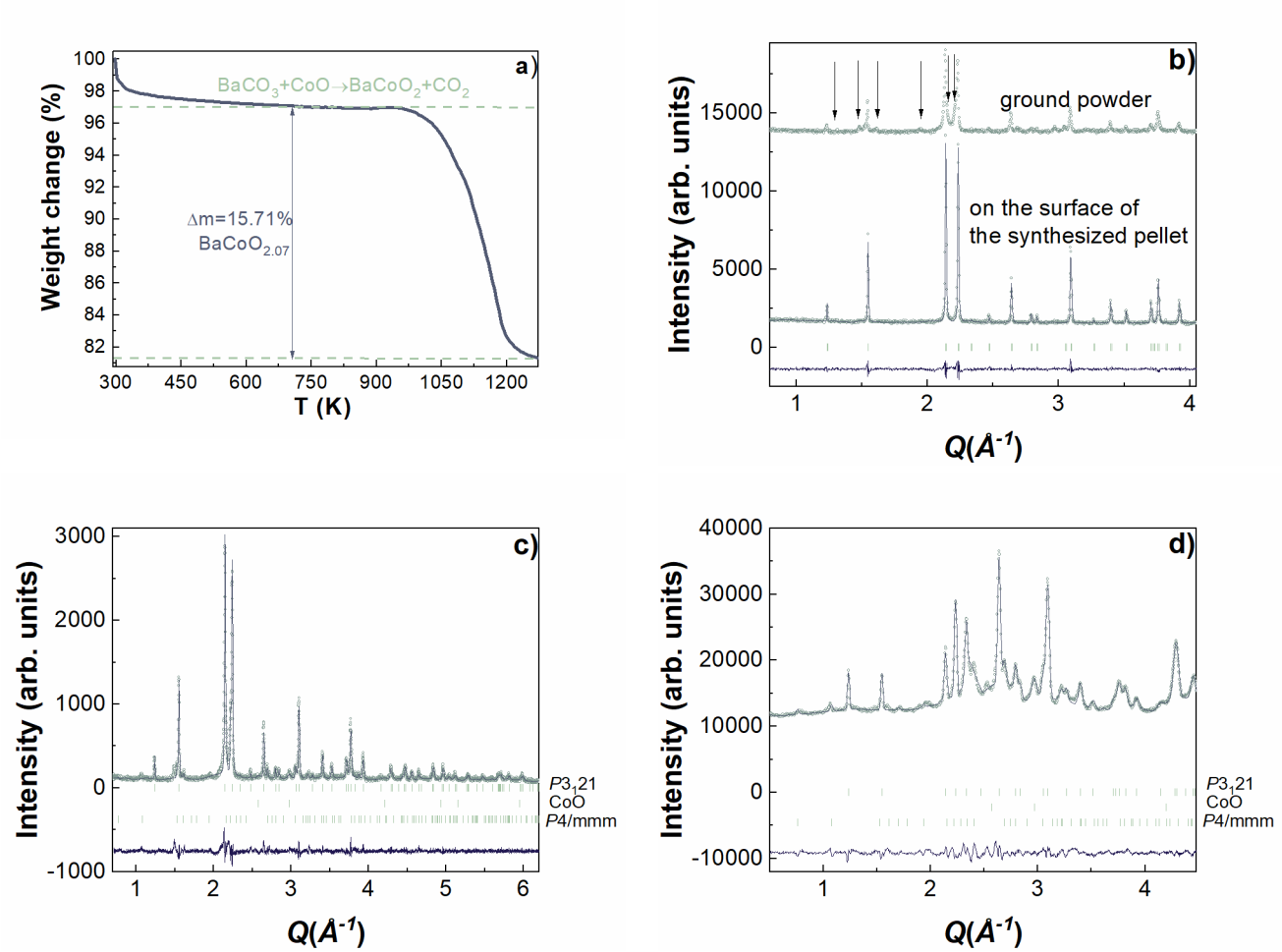

Figure 1: Synthesis and structural characterization of $BaCoO_2$. (a) TGA data from the "in-situ" reaction from precursors, i.e. $BaCO_3$+CoO, under secondary vacuum. (b) Structural data using *K*-Cu_α-radiation from the surface (bottom) and the ground powder (top) of a pellet; on the surface of the pellet, the structure of the single, trigonal $P3_121$ $BaCoO_2$ phase can be refined by the Rietveld method (Bragg R-factor = 4.63 %). Rietveld refinement from bulk powder from (c) X-ray using *K*-$Cu_{\alpha 1}$-radiation (Bragg R-factor: 6.71 %) and (d) neutron diffraction using λ=2.52 Å (Bragg R-factor: 4.09 %) obtained at 400 K. Experimental, simulated data and difference are respectively shown using open dots, gray and blue lines. Vertical ticks indicate the the Bragg reflections of the $P3_121$ $BaCoO_2$, CoO and *P*4/mmm $BaCoO_{2+\delta}$ phases (with their corresponding calculated weight fractions from Rietveld refinement: 77 – 7 and 16 %).

derived trigonal structure[26] with a helicoidally corner-sharing, CoO_4-tetrahedral-framework, Figure S2. However, only the $BaCoO_2$ unit cell parameters have beeen determined and from the similarities between the x-ray diffraction powder patterns, the $BaZnO_2$-type structure with the $P3_121$ space group was proposed[26,38]. Recently, a tetragonal, highly oxygen-deficient metastable phase $BaCoO_{2+\delta}$ with the *P*4/*mmm* space group[39] and another *P*2₁/*m* monoclinic $BaCoO_{2.67}$[40] form derived from the cubic perovskite structure were also reported, Figure S3. The latter structure has three different Co coordination environments, an octahedral, a square pyramidal and a tetrahedral one.

As already proposed by Spitsbergen et al.[26], $BaCoO_2$ could be synthesized under vacuum conditions. Figure 1a shows the thermogravimetric (TGA) data from the *in-situ* reaction from precursors, i.e. $BaCO_3$+CoO, under secondary vacuum, which results from the formation of $BaCoO_2$ and the carbon dioxide loss. The typical, quartz-derived trigonal pure $BaCoO_2$ diffraction pattern can be obtained from the surface of a pellet synthesized using an appropriate protocol under secondary vacuum described in the experimental section, Fig 1b. Additional reflections consistent with a small amount of CoO and the existence of another phase exhibiting tetragonal symmetry are always present when grinding the pellet and are further assigned to the $BaCoO_{2+\delta}$ phase with *P*4/*mmm* space group[39] as indicated by X-ray diffraction and neutron diffraction patterns, Figure 1c and 1d respectively. It is therefore important to note that the mechanism of oxygen release occurs at the interface of the pellet with secondary vacuum atmosphere as the tetragonal phase is absent at the surface of the pellet, i.e. Cu K_α X-rays are strongly absorbed by the barium cobalt oxide pellet and probe only its first micron-surface. $BaCoO_2$ presents an arrangement of intermediate compactness between the quartz and $BaZnO_2$ structures[38], as determined from the ***c***/***a*** unit-cell parameter ratio, the tetrahedral tilt angle δ and the intertetrahedral bridging angle θ, Figure S4 and Table S1, whereas the CoO_4 tetrahedra are found to be slightly distorted (1.906(13)Å and 2.023(14)Å Co-O bonds)[41]. Bond Valence Sum (BVS) information is shown on Table S2 and shows an appropriate value for the cobalt cation charge (1.94(3)). In addition to its non-centrosymmetric space group, the $BaCoO_2$ phase exhibits an antiferromagnetic order above room temperature

with $T_{Néel}$ = 335 K as evidenced by magnetic susceptibility and magnetization measurements, Figure S5. From the Curie-Weiss law fitted between 365 K and 400 K, θ = -573(1) K and μ_{eff} = 4.95(5) μ_B. Our experimental value is very close to the values found for paramagnetic salts containing Co^{2+} ions (μ_{eff} = 4.9 μ_B)[42].

$BaCoO_2$ exhibits a thermally activated conduction process with an activation energy E_a = 520 meV, which would lead to an electrical resistivity similar to BSCF at about 1273 K, Figure S6. Note that our electrical resistivity measurements at ambient temperature are also in qualitative agreement with those reported for cubic $BaCoO_{2.22}$[18], which implies that both reduced phases exhibit similar transport properties. However, the value reported for $BaCoO_{2+\delta}$ ($P4/mmm$ space group) with an electrical resistivity about 10^{-8} ohm.cm contradicts these similarities and is therefore difficult to explain[39]. The comparison of the transport properties with $BaCoO_3$[43] and BSCF[44] is important as $BaCoO_2$/$BaCoO_3$ are parent phases for this solid solution and as the oxygen stoichiometry of BSCF in this temperature range is proposed to be between 2.3 to 2.6 with the cobalt being mostly in the 2+ state[45]. The tetrahedral local environment of Co^{2+} may be of interest for electrocatalytic properties as the corner-sharing CoO_4-tetrahedral network of $YBaCo_4O_7$ was already reported to exhibit enhanced oxygen evolution reaction properties similar to that already observed in BSCF[46]. One could also speculate that oxygen conductivity at high temperature could further participate in the decrease of resistivity in $BaCoO_2$ as found for example for BSCF in N_2/air[44] for which the resistivity was found to be sensitive to the PO_2; such a hypothesis will be comforted later by the oxygen release in BCO above 1023 K, which evidences the oxygen permeation in this temperature range. Therefore, transport properties of $BaCoO_2$ are potentially primordial to understand the conductivity properties of BSCF. Note, finally, that the simulated infrared spectrum of $BaCoO_2$ appears to be in qualitative agreement with the experimental one, Figure S7, and completes therefore the characterization of this compound.

Towards $BaCoO_3$ and reversibly:

TGA measurements of $BaCoO_2$ in an oxygen flux are shown in Fig 2a. Upon heating, two large increases in mass are observed, the inflection points for which are at about 433 K and 548 K. The associated oxygen insertion into the $BaCoO_2$ structural framework continues up to 1009 K with a constant slope to reach a weight change of 5.9%, which would be compatible with a $BaCoO_{2.83}$ stoichiometry. When temperature further increases, two mass decreases occur at about 1103 K and at a temperature beyond 1273 K. Based on these data, one could imagine a TGA experiment showing the reduction of a fully oxidized $BaCoO_{3-\delta}$ phase to $BaCoO_2$ under secondary vacuum as already performed (Figure 1a) to show the reversibility of the reaction and probing therefore the oxygen release. To obtain this BCO compound, a synthesis in oxygen flux close to the temperature of the maximum weight change observed in Figure 2a, i.e. 993 K, was performed and resulted in an almost pure 2H-$BaCoO_{3-\delta}$ phase. Whereas X-ray diffraction data showed an almost single BCO phase, Figure S8a, neutron diffraction data, Figure S8b, indicates the coexistence with the 12H-$BaCoO_{2.6}$ phase with an 87.8/12.2 % weight fraction ratio. Neutron diffraction appears as the appropriate technique to probe the purity of the 2H-$BaCoO_{3-\delta}$ phase due to its stronger sensitivity to the light element oxygen, for which the contribution to scattering is low as compared to barium in X-ray diffraction. It is highly important to note that the coexistence with the 12H-$BaCoO_{2.6}$ phase is probably inherent of such a high temperature synthesis reaction as previous neutron diffraction data from the literature claiming a "2H-$BaCoO_{3-\delta}$ single phase" already presented the two most intense reflection of the $BaCoO_{2.6}$ phase (Figure 1 from this reference)[47] as shown by the arrows about 70 ° (2θ) in Figure S8b.

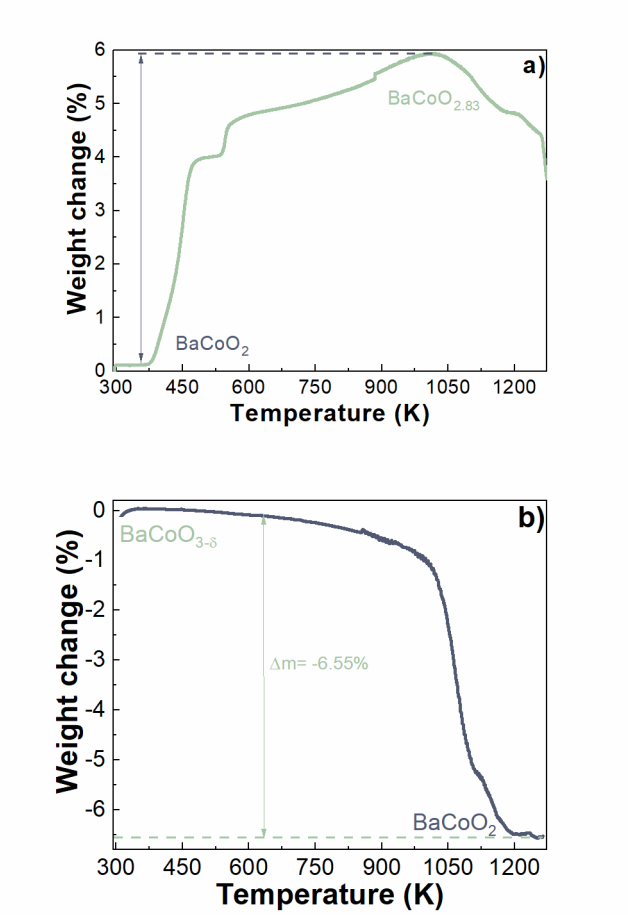

Figure 2: $BaCoO_2 \leftrightarrow BaCoO_{3-\delta}$ probed by TGA. (a) TGA in oxygen atmosphere with a 2.5 K/min ramp. (b) TGA in a vacuum about 5-6.10^{-5} bar with a 2.5 K/min ramp.

Figure 2b shows the TGA data from as synthesized BCO under secondary vacuum up to 1273 K. The inflection point of the single mass-decrease occurs at close to 1073 K and at about 1273 K the resultant oxygen stoichiometry from the mass change observed is associated with a mass loss of 1 entire oxygen atom, which confirms the almost stoichiometric nature of the synthetized $BaCoO_{3-\delta}$ and the resultant $BaCoO_2$ compound under vacuum. The possibility to insert and release such a large amount of oxygen can be considered as a giant oxygen storage capacity (OSC); with 1 oxygen per $BaCoO_2$ it corresponds to an OSC of 4381 µmol O/g which is more than twice the highest reported one in the case of $YBaCo_4O_7$ (2091 µmol O/g)[48]. It is first quite interesting to remark that the previous highest OSC reported was already based on barium cobalt oxide. The observed giant OSC in the present study provides an explanation for the great potential energy storage and conversion devices from BCO-based perovskite and -nanocomposite materials. In the following section, the *in-situ*

structural evolution of $BaCoO_2$/BCO is investigated in order to understand the material's behaviour during OSC.

***In-situ* structural characterization of the oxygen storage/release:**

Figure 3 shows the structural evolution of $BaCoO_2$ as a function of temperature in air by X-ray diffraction, which is consistent with the existence of four different phase

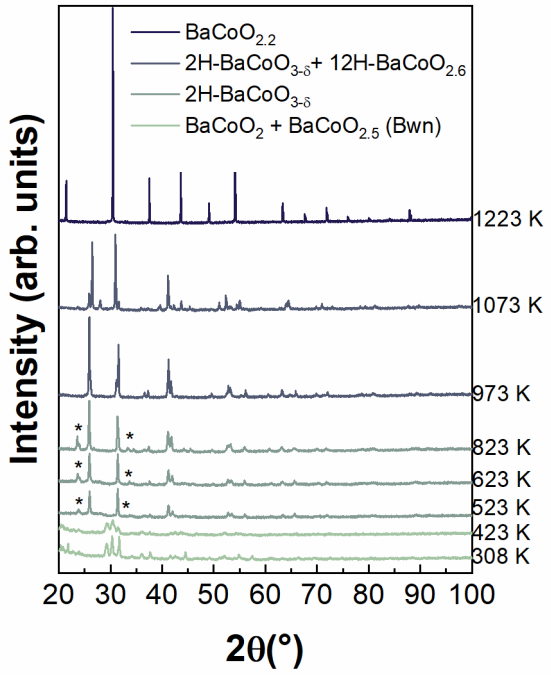

Figure 3: Structural evolution of $BaCoO_2$ as a function of temperature in air by X-ray diffraction.

transitions in the investigated temperature range. $BaCoO_2$ is found to partially transform into $BaCoO_{2.5}$ brownmillerite (Bwn) phase upon heating, a phase which was recently reported[40]. At 523 K, a transition towards the 2H-$BaCoO_{3-\delta}$ phase is observed although one can note some additional reflections marked by (*) which could not be indexed. With additional heating at 973 K, a phase coexistence with $BaCoO_{2.6}$ could be evidenced, while a transformation to the cubic $BaCoO_{2.2}$ phase can easily be observed at 1223 K. Note the gradual sharpening of the reflections with increasing temperatures, which indicates the progressive increase in the domain size during heating. Unfortunately, higher temperatures could not be achieved using this experimental setup. At this stage, it is important to mention that the $BaCoO_2$ phase could potentially be obtained *in-situ* with additional heating as we were able to synthesize it at about 1273-1373 K under an argon atmosphere. In air, $BaCoO_2$ could therefore already oxidize to BCO and back-transform to $BaCoO_2$ in an interesting "oxygen-window temperature range" which is particularly important for many potential energy storage and conversion device applications. However, in the presence of oxygen even the ultra-quench method (e.g. in liquid nitrogen) will induce the reabsorption of oxygen. As previously mentioned, Cu-K_α X-rays are strongly absorbed by barium cobalt oxide and probe only its first micron surface. It is therefore of interest to structurally study OSC properties of bulk $BaCoO_2$/BCO to check if a difference in behavior could be observed between the bulk material and the surface (probed by x-ray diffraction). One can question if all the phases reported in the literature are thermodynamically stable in such a system. For these reasons, an *in-situ* combined (TGA)-neutron diffraction experiment was performed on a large sample volume/mass.

Characterization of $BaCoO_2$ in air by *in-situ* combined TGA-neutron diffraction at high temperature is shown in Fig 4a-4b respectively. Contrary to the X-ray diffraction study, the Bwn structure is not observed upon heating from ambient temperature, Figure 4a. This means that such a phase is probably metastable and may start to be formed and grow from the surface of the material depending on the kinetics. As a consequence, $BaCoO_2$ is found to be surprisingly stable up to 523 K with really low oxygen absorption and a resulting stoichiometry $BaCoO_{2.04}$ at this temperature. $BaCoO_2$ then directly transforms to pure BCO at 523 K. Contrary to the BCO phase synthesized at high temperature, the 2H-$BaCoO_{3-\delta}$ hexagonal structure is obtained as a single phase without the presence of any 12H-$BaCoO_{2.6}$ phase as observed in Figure S8b. More importantly, in the 2H phase, an antiferromagnetic peak compatible with a propagation vector of k = (0,0,1/2) can be identified, Figure S9. The magnetic structure consists of a helix with a magnetic moment in the *ab* plane that rotates 90° along the ***c*** axis. The refined magnetic moment of Co is 0.76(3)μB which is lower than the expected value for Co^{4+} ions in the low-spin state with S=1/2, i.e. m_o=1 μB, due to the high temperature of the refined neutron data (623 K). This structure corresponds to a magnetic space group C_c2. This antiferromagnetic phase is very stable as a function of temperature and is found to disappear at about 700 K. $T_{Néel}$ could not appropriately be determined due to a temperature jump in the furnace used between 705 K and 827 K; as it will be shown latter, the furnace used in the present study was not powerful enough and the regulation of its temperature, which was probably close to its highest power regime unfortunately induced this large temperature increase. Note that such a surprisingly high temperature ordering was already reported in BSCF based on a Mössbauer spectroscopy[49] study with $T_{Néel}$ = 588 K and G-type antiferromagnetic order was determined from a neutron diffraction study[21], which comforts therefore the present result. In the literature for BCO, however, a similar antiferromagnetic order was found with a very low Néel temperature of about 15 K and ferrimagnetic correlations between 15 K and 53 K[47]. Such a huge difference with the reported results can be explained from a phase coexistence of BCO with the 12H-$BaCoO_{2.6}$ ferromagnet[50] in all the previous studies. The way to obtain pure BCO phase appears therefore to oxidize a reduced phase like $BaCoO_2$. Note that a BCO synthesized at high pressure and high temperature was recently reported in the literature[51] with an oxygen content, i.e. $BaCoO_{2.37}$, which lies within the values determined in the present study.

BCO strongly absorbs oxygen in its structure up to the 705-827 K range, for which the furnace used showed an unexpected temperature jump, to reach $BaCoO_{2.84}$ stoichiometry. Note that in the present neutron diffraction study, the use of a λ=2.52 Å wavelength, i.e. with a corresponding resolution up to 1.4 Å, did not permit the oxygen occupation to be refined; this parameter was therefore fixed to the value determined from the TGA measurements in Figure 4b. $BaCoO_{3-\delta}$ exhibits therefore in this study outstanding oxygen storage capacity

with 0.96 ≤ δ ≤ 0.16 in the same structure; in the absence of the furnace-induced temperature jump, stoichiometric pure

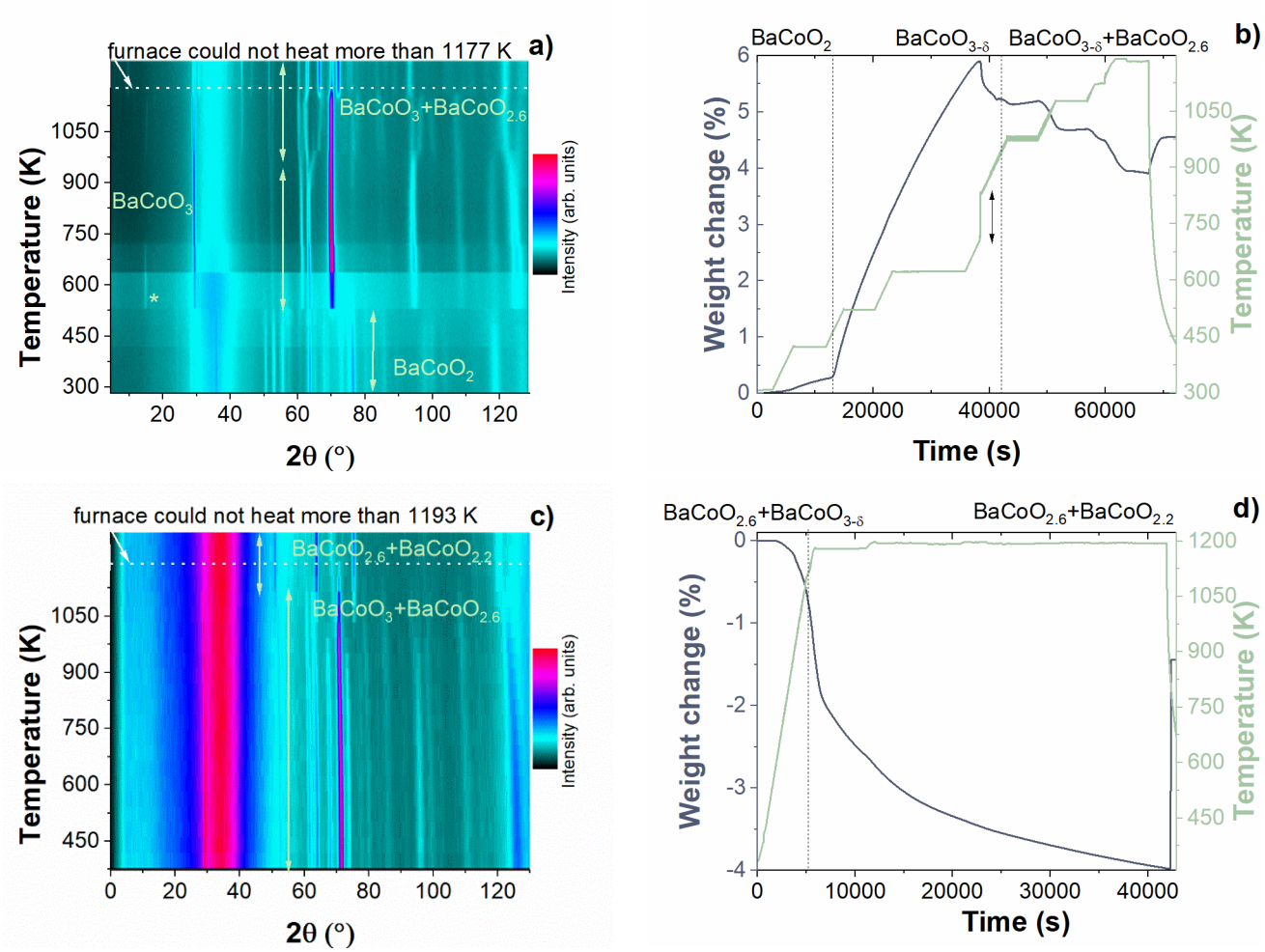

Figure 4: *In-situ* combined TGA - neutron diffraction characterizations of the giant OSC in $BaCoO_2$/BCO. (a) Structural and (b) TGA evolution of $BaCoO_2$ in air; the temperature profile consists of 2 K/min ramps followed by several temperature stabilizations as indicated in the figure. Note a jump in temperature between 705 and 827 K from the used furnace as marked by the double arrow vector. (c) Structural and (d) TGA evolution of BCO in vacuum (10 K/min). In both structural studies, the maximum temperatures reached are indicated due to the furnace limitation; however, neutron data were still collected at this temperature. Stability field of the different phases are indicated. * corresponds to the most intense reflection of the antiferromagnetic phase of BCO defined by k = (0,0,1/2).

BCO (as characterized in Fig 2b) could be obtained. This means that such a phase exhibits unprecedented capacity for oxygen absorption and really acts as an oxygen sponge.

Note that the BVS obtained for BCO in this temperature range are highly interesting as reported in Tables S3 and S4 in the supporting information respectively obtained at 523 and 702 K. Close to the transformation from $BaCoO_2$, the Co-value changes from 1.94 to 3.2 in agreement with the supposed change in oxidation state of the cobalt cation with an associated change in its coordination number from 4 to 5. When the oxygen content reaches its maximum, the BVS Co-value increases up to 3.8 and its coordination number is close to that of a stoichiometric perovskite, i.e. 5.76 compared to 6 for perovskite. This means that oxygen insertion in the BCO phase exhibits a progressive change in the Co-oxidation state from 3+ to 4+.

Additional temperature increases result in oxygen desorption, which is concomitant with the progressive transformation into the 12H-$BaCoO_{2.6}$ phase at about 830-950 K; from the neutron data, it is difficult to estimate the exact temperature of such a transition and the TGA measurements are probably more appropriate to estimate it with the onset of the weight loss as a signature of the phase transition. The transformation from BCO to 12H-$BaCoO_{2.6}$, which both adopt the same $P6_3/mmc$ space group is reconstructive as it induces a clear change in the framework with the appearance of CoO_4 tetrahedra in the latter 12H-phase. However, it looks "continuous" from the neutron data in Figure 4a. Such a property has interesting implications in the reversible oxygen storage/release between these two phases as a continuous behavior without any hysteresis is always targeted to reach high reproducibility for oxygen evolution/reduction reaction applications; Cai *et al.* have recently demonstrated such a scenario by reporting outstanding oxygen carrier capacity with a high stability of hexagonal BCO phases for chemical looping air separation

during 50 cycles at 1148 K[52]. The BCO to 12H-$BaCoO_{2.6}$ transformation could also explain the reasons of the phase coexistence between these two compounds during BCO synthesis in the literature as combined TGA-neutron diffraction data were not previously available to estimate the optimum temperature of interest. Additional temperature increases resulted in an increase in the $BaCoO_{2.6}$/ $BaCoO_{3-\delta}$ phase fraction which reached 70/30 % respectively at the highest temperature (1177 K) with continuous oxygen release, Figure S10; at this temperature the stoichiometry is $BaCoO_{2.56}$. Unfortunately, the furnace did not permit higher temperatures to be reached. When the temperature is quenched to ambient, the final stoichiometry of the experiment is $BaCoO_{2.63}$.

Characterization of BCO under vacuum by *in-situ* combined TGA-neutron diffraction at high temperature is shown in Fig. 4c-4d respectively. As previously mentioned, the starting $BaCoO_{3-\delta}$ compound corresponds to a $BaCoO_{3-\delta}$/$BaCoO_{2.6}$ phase mixture with a (87.8%/12.2%) weight fraction as found from Rietveld refinement, Figure S8b. In this study steeper temperature ramp of 10 K/min was used. When temperature is increasing at about 873 K, weight loss begins to be observed. At about 1123 K, the BCO phase starts to transform to the cubic $BaCoO_{2.2}$ phase, Figure S11. The steep temperature ramp combined with the small domain size and the associated low data quality did not allow us to determine if there is or not an intermediate transformation to the $BaCoO_{2.6}$ phase before that to the cubic $BaCoO_{2.2}$ phase. Again, the furnace could not heat to more than 1193 K, a temperature which was held constant and the following oxygen stoichiometry $BaCoO_{2.39}$ was obtained by TGA.

The previously described *in situ* investigation of the structural evolution highlighted the existence of small domain sizes and low crystal quality. To delve deeper into the structural modifications through the study of local order, we performed Raman spectroscopy, which is a powerful vibrational spectroscopic technique commonly employed to study local order in materials such as ferroelectric relaxors[53] or in an amorphous state[54]. Figure 5 shows the *in situ* Raman spectra of $BaCoO_2$ in air along with the calculated positions of the vibrational modes for $BaCoO_2$/BCO from density functional theory (DFT).

The Raman spectrum of BaCoO2 is in qualitative agreement with the positions of the DFT calculated modes. As the temperature rises up to 573 K, there is a discernible increase in the linewidth due to the reduction in phonon lifetime. The transformation to BCO occurs at 673 K, a temperature which is slightly higher than that previously observed. This phenomenon can be attributed to variations in the thermal history of the present sample compared to the previous ones, which certainly alter the kinetics of the reaction. The shift in the strongest peak to lower wavenumber is related to the increase in coordination of Co. Here again the BCO spectrum is in qualitative agreement with the positions of the modes calculated by DFT. Further temperature increases result in a significant increase in the linewidth as expected due to anharmonicity. This broadening may be associated to a partial transformation to the $BaCoO_{2.6}$ phase as previously found. At 1273 K, only the thermal emission of the compound can be observed without any discernable vibrational features. This is clearly compatible with a transformation to cubic $BaCoO_{2.2}$ ($Pm\bar{3}m$) for which there are no Raman-active vibrational modes based on group theory. Remarkably, the outcomes of this local order investigation significantly reinforce the conclusions drawn in this study.

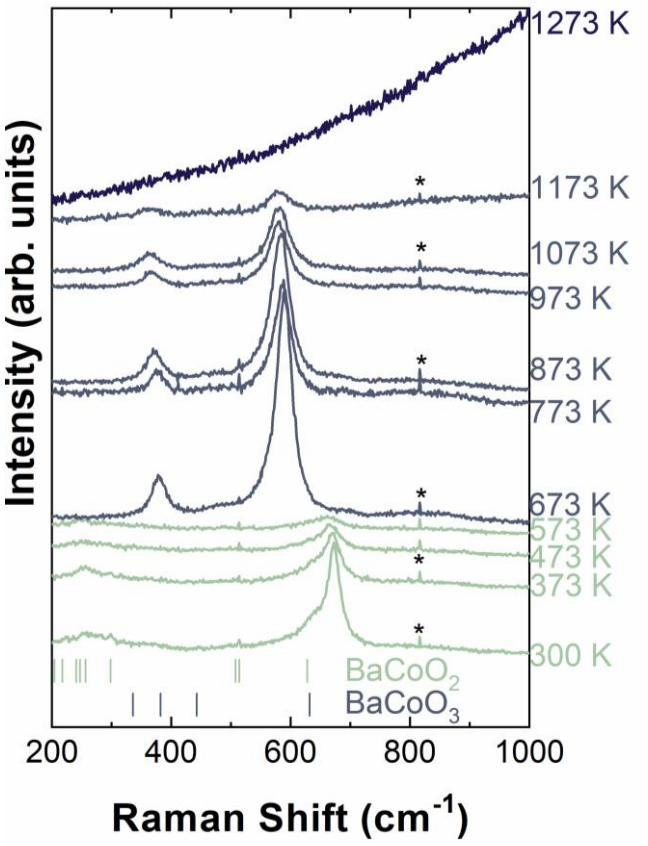

Figure 5: *In situ* Raman spectra of $BaCoO_2$ in air. Vertical ticks indicate the calculated positions of the vibrational modes for $BaCoO_2$ and BCO phases. * are artefact lines.

Figure 6a shows the temperature dependence of the "average atomic volume" (AAV) of $BaCoO_2$/BCO in air/under vacuum[55]. AAV which defines the average volume of atoms occupying a unit cell can be calculated as follows AAV=V/(Z*N) for which V is the unit cell volume, Z is cell formula units and N is the number of atoms in the chemical formula. Such a concept is particularly interesting in the present study as it permits to compare the atomic volume of different stoichiometry in the same graph. The AAV of $BaCoO_2$ in air exhibits an inverse bell-curve profile which is typical for OSC materials, which present their specific oxygen window temperature range first oxidizing with increasing temperature at roughly 575 K and reducing at higher temperatures, i.e. 1230 K in the present case. The data shown in Figure 6a indicates that $BaCoO_2$ with its higher AAV is the most flexible phase observed in the two sequences (air/vacuum) and that BCO is the densest one. Note also that the transition from the cubic $BaCoO_{2.2}$ to the most reduced $BaCoO_2$ phase is suggested to finish the bell-curve in air at about 1250 K, Figure 6a. Finally, Figure 6b shows the structural evolution cycle of $BaCoO_2$/BCO which can be drawn from the present study. In air, the determined transition sequence from neutron/XRD study could be summed up as follows: $BaCoO_2 \rightarrow BaCoO_{3-\delta} \rightarrow BaCoO_{2.6} \rightarrow BaCoO_{2.2}$. As already mentioned $BaCoO_2$ could be either synthesized in an argon atmosphere or under vacuum with the systematic presence of the tetragonal $BaCoO_{2+\delta}$, which from Fig-

ure 1b was found to be more oxidized than the ultimate $BaCoO_2$ trigonal compound. From cubic $BaCoO_{2.2}$, a tiny tetragonal distortion can easily be understood from space-group

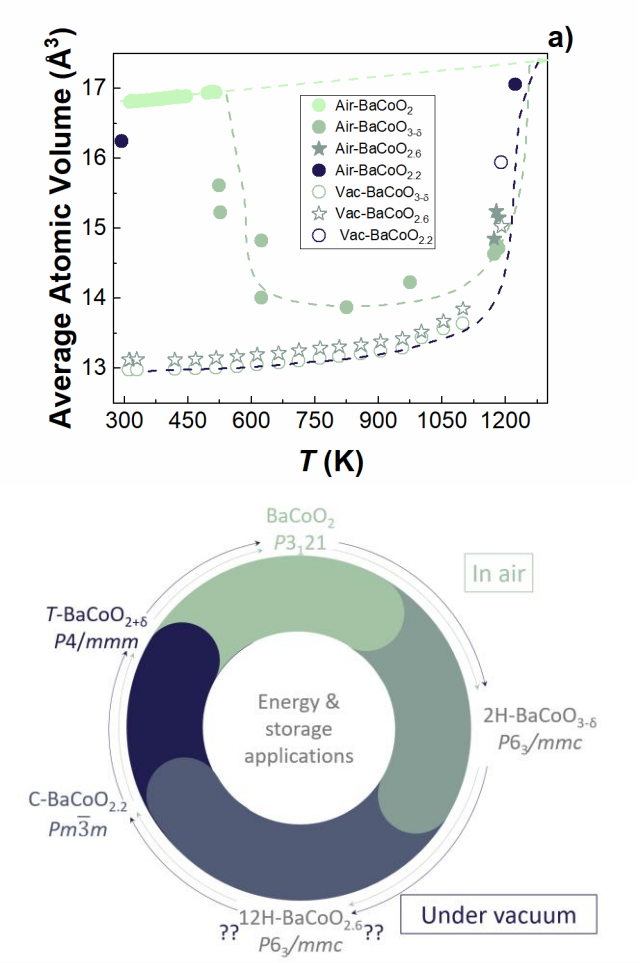

Figure 6: Structural evolution of $BaCoO_2$/BCO. (a) Temperature dependence of the "average atomic volume" of $BaCoO_2$/BCO in air (full symbols) and under vacuum (open symbols) respectively; dashed lines are guide for the eye. (b) Structural evolution cycle of $BaCoO_2$/BCO from the present study "in air" and "under vacuum". Under vacuum the intermediate presence of $BaCoO_{2.6}$ in the path between BCO and $BaCoO_2$ is questioned (??) as described in the text.

theory; the coexistence with the trigonal $BaCoO_2$ is more surprising and is reminiscent of morphotropic phase boundary compounds as already observed in ferroic systems for which the coexistence of tetragonal and rhombohedral symmetry is found to be at the origin of the associated ferroic properties[56-58]. However, it is important to note that all the transformations reported in Figure 6b are reconstructive and do not necessitate space-group relationships. Under vacuum the presence of $BaCoO_{2.6}$ in the path between BCO and $BaCoO_2$ is questioned due to a large temperature ramp combined with small domain size of the transformed compounds, i.e. low crystal quality in the described *in-situ* study. Additional metastable phases could be obtained during this cycle mainly at the surface of the material and depending on the kinetics of the reaction. However, the cycle shown on Figure 6b provides relevant information to understand $BaCoO_2$/BCO energy storage and conversion applications associated with their giant OSC properties which are also at the origin of the oxygen and electron conducting properties of the well-known $Ba_{0.5}Sr_{0.5}Co_{0.8}Fe_{0.2}O_{3-\delta}$ (BSCF) based-perovskite.

CONCLUSIONS

In summary, in this study we synthesized and fully characterized $BaCoO_2$ and succeeded to determine the reversible conversion to $BaCoO_{3-\delta}$. The oxygen nonstoichiometry of this material can therefore be varied from 0 to 1 due to the versatility in the electronic configuration of the metallic Co cations, i.e. oxidation-, spin- and magnetic-state, which defines the fundamental origins of the material's performance. In the present study, cobalt is found to change from the high spin state of the Co^{2+} in $BaCoO_2$ to the low spin state of Co^{4+} in $BaCoO_3$. The $BaCoO_2$/BCO electronic conductivity are found to reach similar values at temperature above 900 K which associated with the giant OSC permit to explain the great potential of BCO-based nanocomposites and BCO-based-perovskite compounds. Note finally that the present study is strongly comforted by recent reports on pure BCO and Ta-doped BCO which showed outstanding properties respectively for efficient electrocatalyst for oxygen evolution reactions[17] and oxygen electrodes for reversible solid oxide electrochemical cells at reduced temperatures[16].

ASSOCIATED CONTENT

Supporting Information includes additional structural, magnetic, resistivity characterizations of the $BaCoO_2$/BCO system.

AUTHOR INFORMATION

Corresponding Author

* ***Jérôme Rouquette*** - ICGM, Univ Montpellier, CNRS, ENSCM, Montpellier, France ; https://orcid.org/0000-0002-6880-1715

Email : jerome.rouquette@umontpellier.fr

Authors

Aliou Diatta - ICGM, Univ Montpellier, CNRS, ENSCM, Montpellier, France.

Email : alioudiata@gmail.com

Claire V. Colin - *Institut Néel, CNRS and Université Grenoble Alpes, BP166, F-38042 Grenoble Cedex 9, France* ; https://orcid.org/0000-0003-1332-7929

Email : claire.colin@neel.cnrs.fr

Romain Viennois ICGM, Univ Montpellier, CNRS, ENSCM, Montpellier, France ; http://orcid.org/0000-0003-4542-2699

Email : romain.viennois@umontpellier.fr

Mickael Beaudhuin - ICGM, Univ Montpellier, CNRS, ENSCM, Montpellier, France ; https://orcid.org/0000-0002-2568-546X

Email : mickael.beaudhuin@umontpellier.fr

Julien Haines - *ICGM, Univ Montpellier, CNRS, ENSCM, Montpellier, France ;* https://orcid.org/0000-0002-7030-3213

Email : julien.haines@umontpellier.fr

Patrick Hermet - *ICGM, Univ Montpellier, CNRS, ENSCM, Montpellier, France ;* https://orcid.org/0000-0001-8312-3740

Email : patrick.hermet@umontpellier.fr

Arie Van der Lee - *IEM, Univ Montpellier, CNRS, ENSCM, Montpellier, France; https://orcid.org/0000-0002-4567-1831*

Email : arie.van-der-lee@umontpellier.fr

Leszek Konczewicz - *L2C, Univ Montpellier, CNRS, Montpellier, France ; Institut of High Pressure Physics, Polish Academy of Sciences, Sokołowska 29/37, 01-142 Warsaw, Poland;* https://orcid.org/0000-0001-6022-7985

Email : leszek.konczewicz@umontpellier.fr

Pascale Armand - *ICGM, Univ Montpellier, CNRS, ENSCM, Montpellier, France ;* https://orcid.org/0000-0001-8312-3740

Email : pascale.armand@umontpellier.fr

Present Addresses

†If an author's address is different than the one given in the affiliation line, this information may be included here.

Author Contributions

The manuscript was written through contributions of all authors. / All authors have given approval to the final version of the manuscript. / ‡These authors contributed equally. (match statement to author names with a symbol)

Funding Sources

Any funds used to support the research of the manuscript should be placed here (per journal style).

Notes

Any additional relevant notes should be placed here.

ACKNOWLEDGMENT

Our warmest thanks go to the CRG-D1B team who developed the neutron beam thermobalance. We would also like to thank the French Neutronics Federation (2FDN), which contributed to the funding of the thermobalance and allocated time to the experiments.

REFERENCES

1 Suntivich, J., May, K. J., Gasteiger, H. A., Goodenough, J. B. & Shao-Horn, Y. A Perovskite Oxide Optimized for Oxygen Evolution Catalysis from Molecular Orbital Principles. *Science* **334**, 1383-1385, doi:10.1126/science.1212858 (2011).

2 Minh, N. Q. CERAMIC FUEL-CELLS. *Journal of the American Ceramic Society* **76**, 563-588, doi:10.1111/j.1151-2916.1993.tb03645.x (1993).

3 Ormerod, R. M. Solid oxide fuel cells. *Chem. Soc. Rev.* **32**, 17-28, doi:10.1039/b105764m (2003).

4 Suntivich, J. *et al.* Design principles for oxygen-reduction activity on perovskite oxide catalysts for fuel cells and metal-air batteries. *Nat. Chem.* **3**, 546-550, doi:10.1038/nchem.1069 (2011).

5 Fabbri, E. *et al.* Dynamic surface self-reconstruction is the key of highly active perovskite nano-electrocatalysts for water splitting. *Nat. Mater.* **16**, 925-+, doi:10.1038/nmat4938 (2017).

6 Sunarso, J., Hashim, S. S., Zhu, N. & Zhou, W. Perovskite oxides applications in high temperature oxygen separation, solid oxide fuel cell and membrane reactor: A review. *Progress in Energy and Combustion Science* **61**, 57-77, doi:10.1016/j.pecs.2017.03.003 (2017).

7 Qasim, M., Ayoub, M., Ghazali, N. A., Aqsha, A. & Ameen, M. Recent Advances and Development of Various Oxygen Carriers for the Chemical Looping Combustion Process: A Review. *Industrial & Engineering Chemistry Research* **60**, 8621-8641, doi:10.1021/acs.iecr.1c01111 (2021).

8 Song, Y. S. *et al.* Self-Assembled Triple-Conducting Nanocomposite as a Superior Protonic Ceramic Fuel Cell Cathode. *Joule* **3**, 2842-2853, doi:10.1016/j.joule.2019.07.004 (2019).

9 Chen, Y. *et al.* A Highly Efficient Multi-phase Catalyst Dramatically Enhances the Rate of Oxygen Reduction. *Joule* **2**, 938-949, doi:10.1016/j.joule.2018.02.008 (2018).

10 He, F. *et al.* Catalytic Self-Assembled Air Electrode for Highly Active and Durable Reversible Protonic Ceramic Electrochemical Cells. *Advanced Functional Materials* **32**, doi:10.1002/adfm.202206756 (2022).

11 Zhou, Y. C. *et al.* An Efficient Bifunctional Air Electrode for Reversible Protonic Ceramic Electrochemical Cells. *Advanced Functional Materials* **31**, doi:10.1002/adfm.202105386 (2021).

12 Kim, J. H. *et al.* Promotion of oxygen reduction reaction on a double perovskite electrode by a water-induced surface modification. *Energy & Environmental Science* **14**, 1506-1516, doi:10.1039/d0ee03283b (2021).

13 Xu, X. M., Su, C. & Shao, Z. P. Fundamental Understanding and Application of Ba0.5Sr0.5Co0.8Fe0.2O3-delta Perovskite in Energy Storage and Conversion: Past, Present, and Future. *Energy & Fuels* **35**, 13585-13609, doi:10.1021/acs.energyfuels.1c02111 (2021).

14 Gushee, B. E., Katz, L. & Ward, R. THE PREPARATION OF A BARIUM COBALT OXIDE

AND OTHER PHASES WITH SIMILAR STRUCTURES. *J. Am. Chem. Soc.* **79**, 5601-5603, doi:10.1021/ja01578a004 (1957).
15 See Methods
16 Kim, J. H. *et al.* An universal oxygen electrode for reversible solid oxide electrochemical cells at reduced temperatures. *Energy & Environmental Science*, doi:10.1039/d2ee04108a (2023).
17 Mahmoudi, E. *et al.* LaCoO3-BaCoO3 porous composites as efficient electrocatalyst for oxygen evolution reaction. *Chemical Engineering Journal* **473**, doi:10.1016/j.cej.2023.144829 (2023).
18 Mentre, O. *et al.* BaCoO2.22: the most oxygen-deficient certified cubic perovskite. *Dalton Transactions* **44**, 10728-10737, doi:10.1039/c4dt03874f (2015).
19 Shao, Z. P. & Haile, S. M. A high-performance cathode for the next generation of solid-oxide fuel cells. *Nature* **431**, 170-173, doi:10.1038/nature02863 (2004).
20 McIntosh, S., Vente, J. F., Haije, W. G., Blank, D. H. A. & Bouwmeester, H. J. M. Structure and oxygen stoichiometry of SrCo0.8Fe0.2O3-delta and Ba0.5Sr0.5Co0.8Fe0.2O3-delta. *Solid State Ion.* **177**, 1737-1742, doi:10.1016/j.ssi.2006.03.041 (2006).
21 McIntosh, S., Vente, J. F., Haije, W. G., Blank, D. H. A. & Bouwmeester, H. J. M. Oxygen stoichiometry and chemical expansion of Ba0.5Sr0.5Co0.8Fe0.2O3-delta measured by in situ neutron diffraction. *Chemistry of Materials* **18**, 2187-2193, doi:10.1021/cm052763x (2006).
22 Wang, F., Nakamura, T., Yashiro, K., Mizusaki, J. & Amezawa, K. The crystal structure, oxygen nonstoichiometry and chemical stability of Ba0.5Sr0.5Co0.8Fe0.2O3-delta (BSCF). *Phys Chem Chem Phys* **16**, 7307-7314, doi:10.1039/c3cp54810d (2014).
23 Mueller, D. N., De Souza, R. A., Yoo, H. I. & Martin, M. Phase Stability and Oxygen Nonstoichiometry of Highly Oxygen-Deficient Perovskite-Type Oxides: A Case Study of (Ba,Sr)(Co,Fe)O3-delta. *Chemistry of Materials* **24**, 269-274, doi:10.1021/cm2033004 (2012).
24 Efimov, K., Xu, Q. A. & Feldhoff, A. Transmission Electron Microscopy Study of Ba0.5Sr0.5Co0.8Fe0.2O3-delta Perovskite Decomposition at Intermediate Temperatures. *Chemistry of Materials* **22**, 5866-5875, doi:10.1021/cm101745v (2010).
25 Zhou, C. *et al.* Low thermal-expansion and high proton uptake for protonic ceramic fuel cell cathode. *Journal of Power Sources* **530**, doi:10.1016/j.jpowsour.2022.231321 (2022).
26 Spitsbergen, U. THE CRYSTAL STRUCTURES OF BAZNO2, BACOO2 AND BAMNO2. *Acta Crystallographica* **13**, 197-198, doi:10.1107/s0365110x60000467 (1960).
27 Rodriguez-Carvajal, J. in *18th Conference on Applied Crystallography.* 30-36 (2001).
28 DIATTA Aliou; Claire V. Colin and ROUQUETTE Jerome. (2019). In-situ BaCoO3-BaCoO2 topotactic reactions probed by neutron diffraction. Institut Laue-Langevin (ILL) doi:10.5291/ILL-DATA.5-24-633,
29 Kresse, G. & Furthmuller, J. Efficiency of ab-initio total energy calculations for metals and semiconductors using a plane-wave basis set. *Computational Materials Science* **6**, 15-50, doi:10.1016/0927-0256(96)00008-0 (1996).
30 Kresse, G. & Hafner, J. Ab initio molecular dynamics for liquid metals. *Phys. Rev. B* **47**, 558-561, doi:10.1103/PhysRevB.47.558 (1993).
31 Perdew, J. P., Burke, K. & Ernzerhof, M. Generalized gradient approximation made simple. *Phys. Rev. Lett.* **77**, 3865-3868, doi:10.1103/PhysRevLett.77.3865 (1996).
32 Kresse, G. & Joubert, D. From ultrasoft pseudopotentials to the projector augmented-wave method. *Phys. Rev. B* **59**, 1758-1775, doi:10.1103/PhysRevB.59.1758 (1999).
33 Monkhorst, H. J. & Pack, J. D. Special points for Brillouin-zone integrations. *Phys. Rev. B* **13**, 5188-5192, doi:10.1103/PhysRevB.13.5188 (1976).
34 Dudarev, S. L., Botton, G. A., Savrasov, S. Y., Humphreys, C. J. & Sutton, A. P. Electron-energy-loss spectra and the structural stability of nickel oxide: An LSDA+U study. *Phys. Rev. B* **57**, 1505-1509, doi:10.1103/PhysRevB.57.1505 (1998).
35 B. Raveau and M. Seikh , Cobalt Oxides: From Crystal Chemistry to Physics , Wiley VCH, 2012
36 Jacobson, A. J. & Hutchison, J. L. AN INVESTIGATION OF THE STRUCTURE OF 12HBACO02.6 BY ELECTRON-MICROSCOPY AND POWDER NEUTRON-DIFFRACTION. *J. Solid State Chem.* **35**, 334-340, doi:10.1016/0022-4596(80)90530-7 (1980).
37 Boulahya, K. *et al.* Ferromagnetism in Ba5Co5O14: A structural, transport, thermal, and magnetic study. *Phys. Rev. B* **71**, doi:10.1103/PhysRevB.71.144402 (2005).
38 Diatta, A., Rouquette, J., Armand, P. & Hermet, P. Density Functional Theory Prediction of the Second Harmonic Generation and Linear Pockels Effect in Trigonal BaZnO2. *J. Phys. Chem. C* **122**, 21277-21283, doi:10.1021/acs.jpcc.8b08174 (2018).
39 Waidha, A. I. *et al.* BaCoO2+: a new highly oxygen deficient perovskite-related phase with unusual Co coordination obtained by high temperature reaction with short reaction times. *Chemical Communications* **55**, 2920-2923, doi:10.1039/c8cc09532a (2019).
40 Waidha, A. I. *et al.* Structural, Magnetic and Catalytic Properties of a New Vacancy Ordered Perovskite Type Barium Cobaltate BaCoO2.67. *Chemistry-a European Journal* **27**, 9763-9767, doi:10.1002/chem.202101167 (2021).
41 See BaCoO2 cif file
42 Blundell, S. *Magnetism in Condensed Matter*. (OUP Oxford, 2001).
43 Yamaura, K. & Cava, R. J. Magnetic, electric and thermoelectric properties of the quasi-1D cobalt oxides Ba(1-x)La(x)CoO3 (x=0, 0.2). *Solid State Commun.* **115**, 301-305, doi:10.1016/s0038-1098(00)00188-5 (2000).
44 Wei, B. *et al.* Thermal and electrical properties of new cathode material Ba0.5Sr0.5Co0.8Fe0.2O3-delta for solid oxide fuel cells. *Electrochem Solid St* **8**, A428-A431, doi:10.1149/1.1951232 (2005).
45 Arnold, M., Xu, Q., Tichelaar, F. D. & Feldhoff, A. Local Charge Disproportion in a High-Performance Perovskite. *Chemistry of Materials* **21**, 635-640, doi:10.1021/cm802779f (2009).
46 Chen, Y. B. *et al.* Enhanced oxygen evolution over dual corner-shared cobalt tetrahedra. *Nat. Commun.* **13**, doi:10.1038/s41467-022-33000-w (2022).
47 Nozaki, H. *et al.* Antiferromagnetic spin structure in BaCoO3 below 15 K determined by neutron and mu+SR. *J Phys Chem Solids* **68**, 2162-2165, doi:10.1016/j.jpcs.2007.08.059 (2007).
48 Karppinen, M. *et al.* Oxygen nonstoichiometry in YBaCo4O7+delta: Large low-temperature oxygen absorption/desorption capability. *Chemistry of Materials* **18**, 490-494, doi:10.1021/cm0523081 (2006).
49 Gaczynski, P. *et al.* A high-temperature Fe-57 Mossbauer study of (Ba0.5Sr0.5)(Co0.8Fe0.2)O3-delta.

Solid State Ion. **369**, doi:10.1016/j.ssi.2021.115659 (2021).

50 Hebert, S., Pralong, V., Pelloquin, D. & Maignan, A. Hexagonal perovskite cobaltites: Unconventional magnetism at low temperature. *Journal of Magnetism and Magnetic Materials* **316**, 394-399, doi:10.1016/j.jmmm.2007.03.143 (2007).

51 Wang, H. Z. *et al.* Impersonating a Superconductor: High-Pressure BaCoO₃, an Insulating Ferromagnet. *J. Am. Chem. Soc.* **145**, 21203-21206, doi:10.1021/jacs.3c08726 (2023).

52 Cai, G. Q. *et al.* BaCoO3-delta perovskite-type oxygen carrier for chemical looping air separation, part I: Determination of oxygen non-stoichiometry and cyclic stability of oxygen carrier. *Separation and Purification Technology* **302**, doi:10.1016/j.seppur.2022.121972 (2022).

53 Al-Zein, A., Hlinka, J., Rouquette, J. & Hehlen, B. Soft Mode Doublet in PbMg1/3Nb2/3O3 Relaxor Investigated with Hyper-Raman Scattering. *Phys. Rev. Lett.* **105**, 017601 doi:10.1103/PhysRevLett.105.017601 (2010).

54 Weigel, C. *et al.* Polarized Raman spectroscopy of v-SiO2 under rare-gas compression. *Phys. Rev. B* **93**, doi:10.1103/PhysRevB.93.224303 (2016).

55 Gao, Q. L. *et al.* Discovering Large Isotropic Negative Thermal Expansion in Framework Compound AgB(CN)(4) via the Concept of Average Atomic Volume. *J. Am. Chem. Soc.* **142**, 6935-6939, doi:10.1021/jacs.0c02188 (2020).

56 Rouquette, J. *et al.* Pressure tuning of the morphotropic phase boundary in piezoelectric lead zirconate titanate. *Phys. Rev. B* **70**, 014108 doi:10.1103/PhysRevB.70.014108 (2004).

57 Rouquette, J. *et al.* Pressure-induced rotation of spontaneous polarization in monoclinic and triclinic PbZr0.52Ti0.48O3. *Phys. Rev. B* **71**, 024112 (2005).

58 Fraysse, G. *et al.* Low-symmetry phases at the tilt boundary of the Pb(Zr(1-x)Ti(x))O(3) solid solution. *Phys. Rev. B* **77**, 064109, doi:10.1103/PhysRevB.77.064109 (2008).

TOC GRAPHIC